TECHNISCHE UNIVERSITÄT WIEN

Bachelor Thesis:

Photoexcitations in a Quantum Dot - Benzene Heterostructure with non-local Coulomb Interactions

---

written by
Benjamin Orthner
Immatriculation Number: 00473828, Study Code: 033 261

supervised by
Univ.Prof. Dr. Karsten Hel
TU Wien, Institute for Solid State Physics

co-supervised by
Univ.Ass. Dr. Anna Kauch
TU Wien, Institute for Solid State Physics

and co-supervised by
Projektass. Paul Worm, MSc
TU Wien, Institute for Solid State Physics

November 16, 2023

Abstract

Solar power is one of the most promising low carbon energy technologies, allowing electricity generation from free and abundant sunlight. With ever-increasing energy demands on top of the looming threat of a climate crisis, innovations in this field are essential. However, progress in conventional silicon-based solar cell technologies has begun to stagnate as they approach their inherent maximum efficiency of 34%, the Shockley-Queisser-limit [1]. Among a few other proposed alternatives, heterostructures of transition metal oxides may present a solution to this problem, as they display an effect called "impact ionisation".

This thesis builds upon previous works [2, 3, 4, 5], which have implemented the Hubbard model to investigate impact ionisation in a small cluster of atoms within oxide heterostructures being excited by a short light pulse. We expand the capabilities of the existing code to include non-local Coulomb interactions and set up the framework needed to allow the investigation of impact ionisation in a system consisting of a quantum dot coupled to a benzene ring. This is motivated by the experimental work [6], where impact ionisation was observed in a similar system. The benzene ring is modelled as a mono-atomic chain with periodic boundary conditions, and the non-local Coulomb interactions are calculated via the Pariser-Parr-Pople method.

Contents

1 Introduction

1.1 Solar Cells

Solar cells are devices that convert radiation energy into electrical energy via the photovoltaic effect. This is most commonly achieved using the doped semiconductor silicon. In order to understand how they work, we must first understand the electron structure of silicon.

In a semiconductor, at $T = 0\,\mathrm{K}$, all electrons occupy the so-called valence band, which is separated from the unoccupied conductance band by an energy gap of $\sim 1\,\mathrm{eV}$. An electron can traverse this gap by absorbing a photon with an energy higher than that of the band gap. This excitation of an electron into the conduction band leads to an increase in the electric current in the material. If the energy of the photon far exceeds that of the gap, the promoted electron bleeds off this excess energy in a process called thermalisation, in which phonons are excited and heat up the material. The excess energy is effectively lost. If the photon's energy is lower than the gap's, it does not get absorbed at all. Because the sun radiates light on a spectrum, all solar cells of this type are subject to an inherent limit in efficiency, the Shockley-Queisser-limit, which under ideal conditions can reach a maximum of about 34% [1].

Various methods do exist that have the potential to overcome this limit. Among these is an effect called "impact ionisation". To a small degree, this effect occurs in most materials and allows for the excess energy of an excited electron to be used in the excitation of a second electron, instead of being lost to thermalisation. The factor deciding which of the two effects dominates is the time scale on which they occur. In semiconductors, relaxation via phonon excitations occurs on a time scale of about $0.1 - 10,\mathrm{ps}$ whereas for impact ionisation, it is about $1 - 100\mathrm{ps}$, thus making the former far more likely. However, in some materials with strongly correlated electron systems, such as oxide heterostructures, the time-scale for impact ionisation can be as low as 10 fs, thus making it the predominant process for electron relaxation [7].

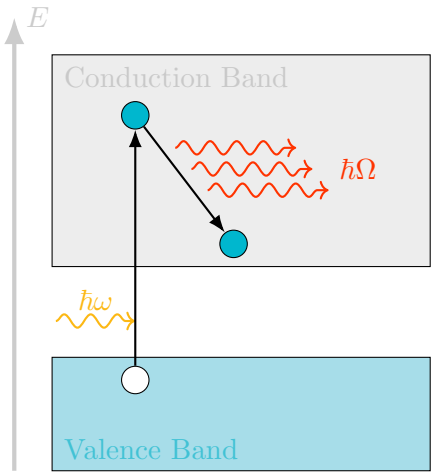

Fig. 1.1 After excitation by a photon, the excess energy of the electron is lost to thermalisation.

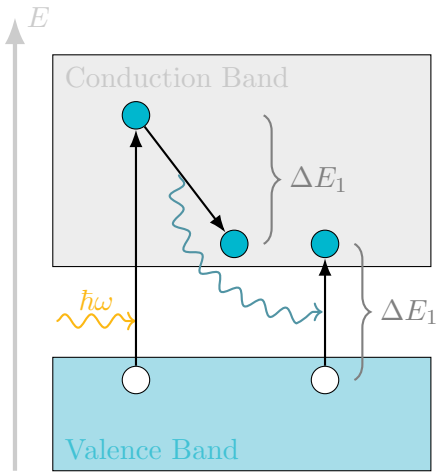

Fig. 1.2 After excitation by a photon, the excess energy is used to excite a second electron to the conduction band via impact ionisation.

1.2 Existing Implementation

In order to study the effects of impact ionisation in solar cells using small Hubbard clusters, a program was developed. The original numerical implementation was by Michael Innerberger [2], and extensions were carried out by Paul Worm [3, 5] and Paul Prauhart [4].

In this section we will only give a brief overview of the main functionality of the code and refer the reader back to the previously mentioned three papers for more details.

1.2.1 Hubbard Model

The Hubbard model was used to study the effect of impact ionisation in a strongly correlated electron system . It describes a system of atoms as a lattice of $N_s \in \mathbb{N}$ sites, each of which can represent the location of at most one spin-up electron and one spin-down electron under the tight-binding approximation. The wave functions that describe such localised electrons are called Wannier-Functions.

Using the second quantisation formalism of quantum mechanics, states of such many-body systems can be described purely by the occupation numbers of each site $n_{i\sigma} = \{0, 1\}$. This allows us to write state vectors as $|\psi\rangle = |n_{1\uparrow} n_{1\downarrow} n_{2\uparrow} n_{2\downarrow} \dots n_{N_s\uparrow} n_{N_s\downarrow}\rangle$. The Hamiltonian can then be expressed using the following two terms

$$\hat{H}_{\text{Hubbard}} = U \sum_i \hat{n}_{i\uparrow} \hat{n}_{i\downarrow} + \sum_{ij\sigma} v_{ji} \hat{c}^\dagger_{i\sigma} \hat{c}_{j\sigma} \tag{1.1}$$

The first corresponds to the repulsive Coulomb interaction U between two electrons with opposite spins located on the same site. The second represents the energy change in the system when an electron hops from site $j \to i$ with hopping amplitude v_{ji}. Here $\hat{c}^\dagger_{i\sigma}, \hat{c}_{j\sigma}$ are the fermionic creation and annihilation operators.

One can interpret the first sum as representing the interaction energy (also sometimes referred to as potential energy) in the system, whereas the second sum for the hoppings represents the system's kinetic energy since it is related to the movement of electrons. This distinction becomes vital in section 2.1, where we introduce non-local Coulomb interactions.

1.2.2 Interaction with Photons

The systems interaction with photons is modelled via a classical electric field pulse

$$\vec{E}(t) = \vec{E}_0 \sin(\omega(t - t_p))\, \mathrm{e}^{-\frac{(t-t_p)^2}{2\sigma^2}} \tag{1.2}$$

with frequency ω, width σ and peak time t_p. This can be integrated into our model by introducing a time-dependent phase factor onto the hopping amplitude in a method called Peierl's substitution [8].

$$v_{ij} \to v_{ij}(t) = v_{ij} \exp\left(i \frac{e}{\hbar} \int_{\vec{R}_i}^{\vec{R}_j} \vec{A}(\vec{r}, t) d\vec{r} \right) \tag{1.3}$$

Here $\vec{A}$ is the electromagnetic vector potential which, in a gauge where the scalar potential vanishes, can be expressed via $\vec{E}(t) = -\partial_t \vec{A}(t)$. Using an approximation for the integral in (1.3) and the equation (1.2), one arrives at

$$v_{ij} \approx v_{ij} \exp\left(ia[\cos(\omega(t - t_p)) - b] e^{-\frac{(t-t_p)^2}{2\sigma^2}} \right) \tag{1.4}$$

where a and b are tunable parameters.

1.2.3 Time-Evolution

Our main interest is to investigate impact ionisation in the system after being exposed to the electric field pulse. Prior to this work, it was achieved by looking at the double occupation observable $\langle \hat{d}(t) \rangle = \langle \hat{n}_{i\uparrow}(t) \hat{n}_{i\downarrow}(t) \rangle$ since the rise of its mean value after initial excitation was an indicator for impact ionisation. In order to compute this quantity, we need the ability to time-evolve any initial state $|\psi(t=0)\rangle = |\psi_0\rangle$ of the system. Using the time-dependent Schrödinger equation

$$i\hbar \frac{\partial}{\partial t} |\psi(t)\rangle = \hat{H}(t) |\psi(t)\rangle \tag{1.5}$$

the time evolution can be computed as

$$|\psi(t)\rangle = \mathcal{T} \exp\left(-\frac{i}{\hbar} \int_0^t H(t')dt' \right) |\psi_0\rangle \tag{1.6}$$

where $\mathcal{T}$ is the time-ordering operator. By numerically dividing t into m small time steps τ, it is justified to use Magnus-expansion [9] of order zero and thus neglect the time-ordering operator. Assuming the time steps are small enough, we can approximate the integral in (1.5) over one time step using the midpoint rule. This leads to the following recursive formula

$$|\psi(m\tau + \tau)\rangle = \exp\left(-\frac{i}{\hbar} H\left(m\tau + \frac{\tau}{2} \right) \right) |\psi(m\tau)\rangle \,. \tag{1.7}$$

This can be computed using the Krylov matrix exponential method [2].

1.2.4 Finding the Initial State

We mainly concern ourselves with half-filled systems when studying impact ionisation, where the number of spin-up and spin-down electrons are the same. The number of electrons is a conserved property of the systems and does not change over time.

It is assumed that before the electric field pulse, the system is in thermal equilibrium and occupies the state with the lowest energy (the ground state). To find this state numerically, a variant of the power iteration method was implemented [2]. From a randomly initialised starting state, it iteratively computes the eigenenergy with the largest absolute value and its corresponding eigenstate, thus recursively converging to the ground state.

1.2.5 Memory Management

The predominant limitation of this implementation is the memory it requires. For a system with N_s sites and a fixed number of electrons, the dimension of its Hilbert space, i.e. the number of linearly independent states, is given by

$$\dim\left[\mathcal{H}_{n_\downarrow}^{n_\uparrow}(N_s)\right] = \binom{N_s}{n_\uparrow} \binom{N_s}{n_\downarrow} \tag{1.8}$$

which for a half-filled system with 14 sites is about 12×10^6. A Hamiltonian matrix of that size, with elements of the data type double, would take over 1000 Terabytes of memory. However, due to the Hamiltonian being made up of mostly zeros, it can be stored and manipulated in a highly compressed sparse matrix format [2], substantially reducing the memory needs.

The states of the system are stored as integers whose binary representations correspond to the occupation configuration of the sites. Actions on these states like creation, annihilation and hoppings have been implemented as bitwise operations.

With all these data-saving measures in place, it was possible to compute the time evolution of 2D square lattices and chains of up to 14 sites, above which memory becomes the limiting factor once again.

1.2.6 Spectral Functions

One way of obtaining information about the states of a system is via spectral functions $A(\omega, t)$. They provide insight into which states and energies the electrons in the system can occupy and thus also tell us about the energies required for optical electron transitions to occur. The existing codebase offers two methods of computing spectral functions [10]:

Lehmann Spectra

Implemented by M. Innerberger in [2], the Lehmann representation of the spectral function gives the equilibrium, i.e. time-independent, spectrum of the system.

$$A(E) = \sum_{i,\sigma} \sum_{|\phi\rangle} \left(\left| \left\langle \phi \left| \hat{c}_{i\sigma}^\dagger \right| \psi_0 \right\rangle \right|^2 \delta\left(E - E_{|\phi\rangle} + E_0\right) + \left| \langle \phi \left| \hat{c}_{i\sigma} \right| \psi_0 \rangle \right|^2 \delta\left(E + E_{|\phi\rangle} - E_0\right) \right) \tag{1.9}$$

Where $\{|\phi\rangle\}$ is an eigenbasis of $\mathcal{H}(N_s)$ with respective energy $E_{|\phi\rangle}$, and $|\psi_0\rangle$ is the ground state of $\hat{H}$ with energy E_0.

It is quick and straightforward to generate with the existing code and produces numerically elegant results. However, because it is pretty memory intensive, it can not handle systems with a large number of sites. This, together with the fact that we can not investigate the time dependence of the spectrum, prompted the implementation of another way to calculate the non-equilibrium spectral function.

Fourier Transforms of Non-Equilibrium Green's Functions

Initially implemented by P. Worm [3], with efficiency improvements by P. Prauhart [4], the one-particle non-equilibrium greens function $G_{ij\sigma}(t, t')$ can be used to compute the non-equilibrium spectral function $A_{ij\sigma}(\omega, t)$, via forward Fourier transformation.

$$G_{ij\sigma}^{<}\left(t, t'\right) = \mathrm{i} \left\langle \psi\left(t'\right) \left| \hat{c}_{j\sigma}^\dagger \mathcal{T} e^{-\mathrm{i}\int_t^{t'} H(\tau)\mathrm{d}\tau} \hat{c}_{i\sigma} \right| \psi(t) \right\rangle \tag{1.10}$$

$$G_{ij\sigma}^{>}\left(t, t'\right) = \mathrm{i} \left\langle \psi\left(t'\right) \left| \hat{c}_{j\sigma} \mathcal{T} e^{-\mathrm{i}\int_t^{t'} H(\tau)\mathrm{d}\tau} \hat{c}_{i\sigma}^\dagger \right| \psi(t) \right\rangle \tag{1.11}$$

$$A_{ij\sigma}^{\lessgtr} = \frac{1}{\pi} \operatorname{Im} \int_0^\infty \mathrm{e}^{i\omega t_{rel}} \, G_{ij\sigma}^{\lessgtr}(t, t + t_{rel}) dt_{rel} \tag{1.12}$$

A simple interpretation of the definition in (1.10) is that an electron with spin σ is removed from site i of the system at time t, the system is time evolved to t', and then the electron is added back at site j. $G_{ij\sigma}^{<}$ is then proportional to the probability that this system is in the same state as a system at time t' where the electron was never removed. The exact implementation is elaborated on in [3].

Obtaining spectral functions using the existing code

In the current state of the code, the Lehmann spectrum can be generated automatically and is output as a .dat file containing columns of values of $A(\omega)$ for each site.

The Green's function is also output as a .dat file with columns containing complex number values of $G(t, t' = t_0)$ for each site. In order to obtain the spectral function from this, one needs to perform the Fourier transform of this data manually, using (1.12). There is currently no existing function in the codebase that handles this automatically. In order to obtain more usable, less noisy results, one should, prior to the Fourier transform, multiply G with a dampening factor $e^{-\epsilon(t-t_0)}$, which effectively acts as a Lorentzian broadening in frequency space [10]. To achieve a higher frequency/energy resolution, one can additionally zero-pad the domain before performing the Fourier transform.

2 New Implementations

2.1 Non-local Coulomb Interactions

One of the goals of this thesis is to expand the capabilities of the existing code to include non-local Coulomb interactions. This will allow for a more true to life representation of electron systems. In the case of a benzene ring, non-local interactions play a vital role and are necessary if one hopes to reproduce experimental results.

In the existing implementation, the on-site repulsive Coulomb force is accounted for in the Hamiltonian as

$$\hat{H} = \underbrace{U \sum_i \hat{n}_{i\uparrow}\hat{n}_{i\downarrow} + \sum_{i\sigma} v_{ii}\hat{c}^\dagger_{i\sigma}\hat{c}_{i\sigma}}_{\text{Interaction Energy}} + \underbrace{\sum_{i\neq j,\,\sigma} v_{ji}\hat{c}^\dagger_{i\sigma}\hat{c}_{j\sigma}}_{\text{Kinetic Energy}}. \tag{2.1}$$

The extension to nonlocal Coulomb interactions follows naturally as

$$\hat{H} = \sum_{ij\sigma\sigma'} U_{ij\sigma\sigma'}\hat{n}_{i\sigma}\hat{n}_{j\sigma'} + \sum_{i\sigma} v_{ii}\hat{c}^\dagger_{i\sigma}\hat{c}_{i\sigma} + \sum_{i\neq j,\,\sigma} v_{ji}\hat{c}^\dagger_{i\sigma}\hat{c}_{j\sigma}. \tag{2.2}$$

Because only the mutual orientation of the spins σ and σ' can have physical effects, we can split $U_{ij\sigma\sigma'}$ into two $N_s \times N_s$ matrices $U_{ij}^{\text{same-spin}}$ and $U_{ij}^{\text{opp-spin}}$. These must be generated for each system geometry and then be passed as parameters to the Hamiltonian assembly routine. For all results shown in this thesis, $U^{\text{same-spin}}$ and $U^{\text{opp-spin}}$ have been chosen to be identical in their off-diagonal elements. Due to the Pauli exclusion principle, the diagonal elements of $U^{\text{same-spin}}$ must be set to 0, as two electrons with equal spins can not occupy the same site. An example of these matrices can be seen in Fig. 2.5

2.1.1 Electron-Hole Symmetry and Chemical Potential

Local U

In the form (2.3), the Hamiltonian changes differently upon the addition of an electron compared to the addition of a hole. However, it will later prove to be rather useful to have the Hamiltonian be electron-hole symmetric and ideally take the following form

$$\hat{H} = U \sum_i \left(\hat{n}_{i\uparrow} - \frac{1}{2}\right)\left(\hat{n}_{i\downarrow} - \frac{1}{2}\right) + \sum_{i\neq j,\,\sigma} v_{ji}\hat{c}^\dagger_{i\sigma}\hat{c}_{j\sigma}. \tag{2.3}$$

Unfortunately, the numerical implementation of (2.1) is less practical. However, we can alternatively achieve electron-hole symmetry while still using (2.1) by setting the value of the local potential to $v_{ii} = -U/2$.

Non-Local U

The same thing can be achieved for the Hamiltonian with Non-Local Coulomb interactions (2.2) by again making a particular choice of local potential.

$$v_{ii} = -\frac{1}{2}\sum_j \left(U_{ij}^{\text{opp-spin}} + U_{ij}^{\text{same-spin}}\right) \tag{2.4}$$

One can think of this sum as a sum over all the U-matrix elements in the row corresponding to the site i.

Pariser-Parr-Pople Model

The Pariser-Parr-Pople model (PPP) aims to simplify the Hamiltonian of single-band π-electron systems, such as the one of the molecule benzene, to a single p_z orbital form. Its Hamiltonian in electron-hole symmetric form is

$$\mathcal{H}_{PPP} = \underbrace{-t \sum_{\langle ij\rangle\sigma} \left(\hat{c}^\dagger_{i\sigma}\hat{c}_{j\sigma} + h.c.\right)}_{\text{hopping terms}} + \underbrace{U \sum_i \left(\hat{n}_{i\uparrow} - \frac{1}{2}\right)\left(\hat{n}_{i\downarrow} - \frac{1}{2}\right)}_{\text{local Coulomb interaction}} + \underbrace{\frac{1}{2}\sum_{i\neq j} U_{ij}\Big(\hat{n}_i - 1\Big)\Big(\hat{n}_i - 1\Big)}_{\text{non-Local Coulomb interactions}} \tag{2.5}$$

Here $\langle\cdots\rangle$ indicates nearest neighbour hoppings and $\hat{n}_i = \hat{n}_{i\uparrow} + \hat{n}_{i\downarrow}$

In the PPP model, the energy of the non-local Coulomb interaction is calculated using the Ohno parametrisation of the Coulomb interaction [11, 12]

$$U_{ij} = \frac{U}{\sqrt{1 + \alpha|r_{ij}|^2}} \quad \text{where} \quad \alpha = \left(\frac{4\pi\varepsilon_0 U}{e^2}\right)^2 \tag{2.6}$$

and $|r_{ij}|$ is the distance between two sites. This ensures that at long ranges, $r_{ij} \to \infty$, U_{ij} gives the standard Coulomb interaction energy, and at short ranges, $r_{ij} \to 0$, we get the on-site Coulomb interaction $U_{ij} = U_{ii} =: U$

2.1.2 Interaction Energy as a Measure for Impact Ionisation

In the preceding works [2, 3, 5, 4], impact ionisation was studied by looking at how the expectation value of the "site averaged double occupation" changed over time after the initial excitation by the light pulse.

$$\left\langle \hat{d}(t) \right\rangle = \frac{1}{N_s}\sum_i \langle \hat{n}_{i\uparrow}(t)\hat{n}_{i\downarrow}(t)\rangle \tag{2.7}$$

However, the use of this observable was only valid because it happened to be proportional to the interaction energy term in the system's Hamiltonian (2.1). The true measure for impact ionisation is the conversion rate of the system's kinetic energy to its interaction energy for constant total energy.

In a sense, this is the very definition of impact ionisation. In ordinary systems, any excess kinetic energy is lost to phonon excitations. Converting this kinetic energy into interaction energy, for example by promoting another electron to a higher energy level, is what we call impact ionisation.

For a Hamiltonian with non-local Coulomb interactions (2.2), the proportionality between double occupation and interaction energy is lost. Thus a new function was implemented that calculates the site-averaged expectation value of the interaction energy at every time step.

$$\left\langle \hat{E}_{\text{int}}(t) \right\rangle = \frac{1}{N_s}\sum_{ij\sigma\sigma'} \left\langle U_{ij\sigma\sigma'}\hat{n}_{i\sigma}(t)\hat{n}_{j\sigma'}(t)\right\rangle + \sum_{i\sigma}\left\langle v_{ii}\hat{c}^\dagger_{i\sigma}\hat{c}_{i\sigma}\right\rangle \tag{2.8}$$

In the state basis, where each basis vector represents a possible electron configuration, all interaction energy contributions (2.8) lie on the diagonal of the Hamiltonian because there are no electron hoppings involved. Thus in order to implement the calculation of (2.8) in the code, we first extract the diagonal elements of the Hamiltonian $\vec{H}_{diag}$ from its sparse representation, then, at every time step, compute the observable

$$\left\langle \hat{E}_{\text{int}}(t) \right\rangle = \vec{v}^\dagger(t)\left(\vec{H}_{diag} \odot \vec{v}(t)\right) \tag{2.9}$$

where $\vec{v}(t)$ is the state vector of the system at time t and $\odot$ represents component-wise vector multiplication. This is similar to the observable computations shown in [2].

Note that the local potential terms v_{ii} are also included in the Hamiltonian's diagonal.

2.2 Quantum Dot

Quantum dots (QDs) are nanoscopic semiconducting particles that display interesting quantum mechanical effects. Due to their small size, the energy levels of the electrons within them become quantized, much like in atoms. Unlike atoms however, the size of QDs can be chosen arbitrarily, making their absorption spectra highly tunable. Together with cost-effective manufacturing processes this makes QDs an enticing candidate for new photovoltaic technologies.

Their high efficiency in energy conversion has been shown experimentally, and impact ionisation has been proposed as an explanation [13]. In this work we first implement a quantum dot into our model, and investigate whether it can facilitate impact ionisation. Subsequently we couple the quantum dot to a larger molecule, benzene in this case, and investigate the effect of this on impact ionisation. This is motivated by the experimental work done in [6] where impact ionisation was seen in such a system.

2.2.1 Geometry

In implementing quantum dots, one of two choices had to be made. Either we implement a new type of site, with multiple energy levels, or we model the quantum dot as a particular arrangement of sites, which we engineer to have the desired effective energy levels. The latter option requires less alterations to the existing code and thus was chosen.

For all the computations done in this work the QD is modelled as a 2×2 lattice of sites, with the following horizontal, vertical and diagonal hopping amplitudes: $v_h = v_v = 1$, $v_d = 0$.

In order to be consistent with the model used for the Benzene ring, the non-local Coulomb interactions for the QD are also calculated using the PPP model as described in section 2.1.1. The distances used in the Ohno function, shown in Fig. 2.1, were calculated by choosing the lattice constant to be equal to the $C-C$ bond length $d = 1.4\,\text{Å}$. This does not necessarily have a physical basis, but for now it provides sufficient flexibility to engineer the desired spectrum by varying the on-site Coulomb interaction U, which is shown in section 3.1.1.

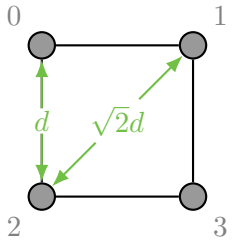

Fig. 2.1 Distances used in Ohno function (2.6) to calculate the Coulomb potential U_{ij}. With $d = 1.4\,\text{Å}$

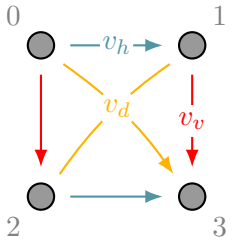

Fig. 2.2 Possible hoppings between QD sites. Arrow direction indicates the direction in which the sign of the imaginary part of the hopping amplitude is positive.

2.2.2 Light pulse direction and hopping time dependence

For every geometry, it is necessary to define a function that explicitly determines whether or not the hopping amplitude v_{ij} between any two sites i and j is time-dependent, i.e. is modified by the light pulse.

This depends on the direction of the light pulse, which is always along the diagonal coming from the top left for our implementation. Any hoppings perpendicular to the pulse direction will remain constant over time and are thus not time-dependent.

The sign of the imaginary parts of the hopping amplitudes is positive for hoppings parallel to the pulse direction and negative for hoppings perpendicular to the pulse direction. By labelling

the sites in lexicographical order, as shown in Fig. 2.2, we ensure that all hoppings from sites $i \to j$ have the same sign as $(j-i)$. The positive directions of the imaginary parts of the hopping amplitudes are indicated in Fig. 2.2 by arrowheads. The diagonal hopping between sites 1 and 2 has no direction shown because, in our case, it is perpendicular to the light pulse and will have no effect regardless.

2.3 Benzene Ring

2.3.1 Hexagonal Geometry

We model the Benzene ring as a 6-site chain with periodic boundary conditions. This has the benefit that it is simple to implement in the existing framework, as a 6x1 lattice with an extra hopping between sites 0 and 5.

The energies of the non-local Coulomb interactions U_{ij} are calculated using the Ohno interpolation (2.6). The distances $|r_{ij}|$ are calculated using the C-C bond length in the benzene molecule, $d = 1.40\,\text{Å}$, and its hexagonal geometry, shown in Fig. 2.3

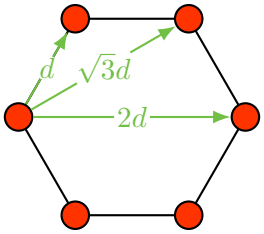

Fig. 2.3 Interatomic distances in Benzene ($d = 1.40\,\text{Å}$)

2.3.2 Hopping amplitudes

One problem with modelling the benzene ring as a chain is that we lose the orientations of the bonds connecting neighbouring sites relative to the light pulse direction. This leads to an inaccuracy in the angle-dependent time dependence of the hoppings between the sites, as illustrated in Fig. 2.4. However, by comparing the results with those of another group, where the orientation was taken into account, we saw only negligible differences in the results and thus choose to move forward with this model.

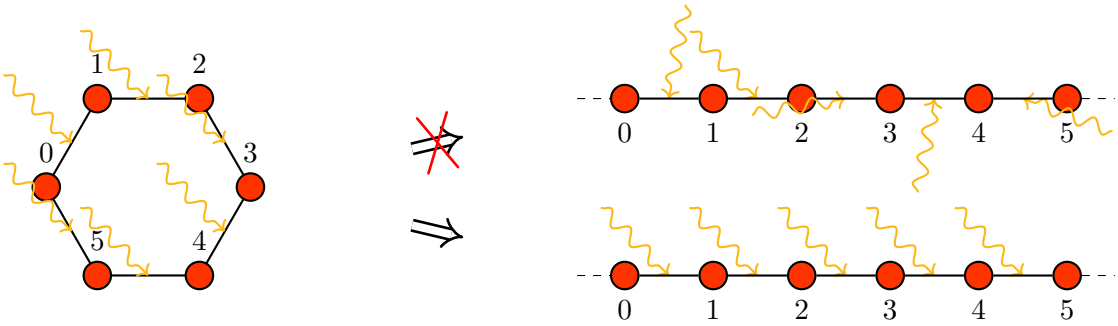

Fig. 2.4 Discrepancy in light pulse orientations relative to sites when modelling benzene as a 1D chain with periodic boundary conditions

2.4 Coupling QD-Benzene

The coupled QD-Benzene system combines the above two systems with an extra hopping from all QD sites to a single benzene site. Again the Coulomb interactions are calculated via the Ohno interpolation and stored in the U matrices. The distances used in the calculations for the U-matrix elements are shown in Fig. 2.5. The hopping amplitudes are the same as in the isolated systems with the addition of a parameter v_c, representing the hopping between the QD and the benzene ring. By setting $v_c = 0$ we would expect to see the same spectra as for the isolated system. As was alluded to in 2.1.1 the on-site hopping term (local potential) v_{ii} differs for Benzene and QD sites and must thus be calculated separately. The hopping matrix is shown in Fig. 2.6

For now we only investigate how the system responds to the light pulse only interacting with the QD sites. Thus we set all the benzene hoppings and the hoppings between the QD and benzene to be non-time dependent.

	0	1	2	3	4	5	6	7	8	9
0		1	1	$\sqrt{2}$	-	-	-	-	-	-
1	1		$\sqrt{2}$	1	-	-	-	-	-	-
2	1	$\sqrt{2}$		1	-	-	-	-	-	-
3	$\sqrt{2}$	1	1		-	-	-	-	-	-
4	-	-	-	-		1	$\sqrt{3}$	2	$\sqrt{3}$	1
5	-	-	-	-	1		1	$\sqrt{3}$	2	$\sqrt{3}$
6	-	-	-	-	$\sqrt{3}$	1		1	$\sqrt{3}$	2
7	-	-	-	-	2	$\sqrt{3}$	1		1	$\sqrt{3}$
8	-	-	-	-	$\sqrt{3}$	2	$\sqrt{3}$	1		1
9	-	-	-	-	1	$\sqrt{3}$	2	$\sqrt{3}$	1	

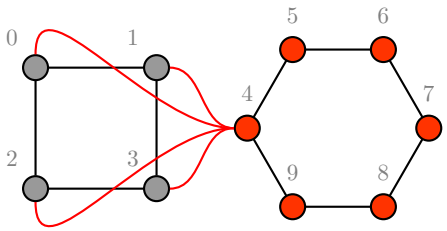

– for equal spin matrix
1 for opposite spin matrix

- We assume strong shielding between benzene and quantum dot
⇒ no Coulomb interaction

Fig. 2.5 Structure of the coulomb interaction matrices $U_{ij\sigma\sigma'}$. Each entry represents the distance between two sites as a multiple of the C-C bond length $d = 1.40\,\text{Å}$. The U_{ij} matrices can be constructed by applying the Ohno function 2.6 to each entry in the table. Note that a dash implies an infinite distance (- $= \infty$).

	0	1	2	3	4	5	6	7	8	9
0	v_{ii}^{qd}	v_h	v_v	v_d	v_c	0	0	0	0	0
1	v_h	v_{ii}^{qd}	v_d	v_v	v_c	0	0	0	0	0
2	v_v	v_d	v_{ii}^{qd}	v_h	v_c	0	0	0	0	0
3	v_d	v_v	v_h	v_{ii}^{qd}	v_c	0	0	0	0	0
4	v_c	v_c	v_c	v_c	v_{ii}^{b}	v_h	0	0	0	v_h
5	0	0	0	0	v_h	v_{ii}^{b}	v_h	0	0	0
6	0	0	0	0	0	v_h	v_{ii}^{b}	v_h	0	0
7	0	0	0	0	0	0	v_h	v_{ii}^{b}	v_h	0
8	0	0	0	0	0	0	0	v_h	v_{ii}^{b}	v_h
9	0	0	0	0	v_h	0	0	0	v_h	v_{ii}^{b}

Fig. 2.6 Hopping elements between sites, as multiples of the C-C bond length ($d = 1.40\,\text{Å}$)

3 Results and Conclusion

3.1 Isolated Quantum Dot

3.1.1 Engineering the spectrum

To encourage impact ionisation, we engineer the quantum dot to have 4 equally spaced energy levels. As shown in Fig. 3.1 (and Fig 1.2), this allows for an electron from the lower Hubbard band to be excited into the most energetic state and, during its subsequent decay, to promote a second electron over the Mott gap.

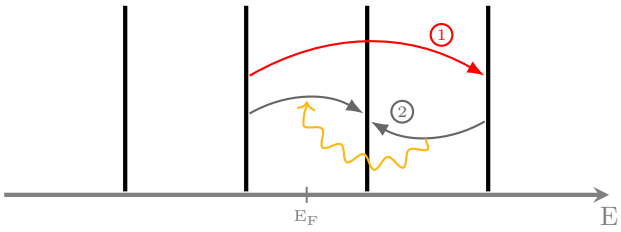

Fig. 3.1 Illustration of why equally spaced energy levels encourage impact ionisation through Coulomb interactions.
1. An electron is promoted by two energy levels.
2. The promoted electron gives up half its energy to promote a second electron (squiggly line)

The main parameter that needs to be tuned to achieve such a spectrum is the on-site Coulomb potential $U \equiv U_{ii}$, as it is directly responsible for the size of the Mott gap. A loop was set up to compute the Lehmann spectrum of the system for a range of values of U. The mean differences in the spacings between the peaks were extracted and plotted as a function of the Coulomb potential. By regressing a line to this data, we were then able to determine that $U = 2.41$ produced the desired energy level spacing for our choice of parameters. Fig. 3.2 shows a series of Lehmann spectra produced in this process as well as the final, equally spaced spectrum.

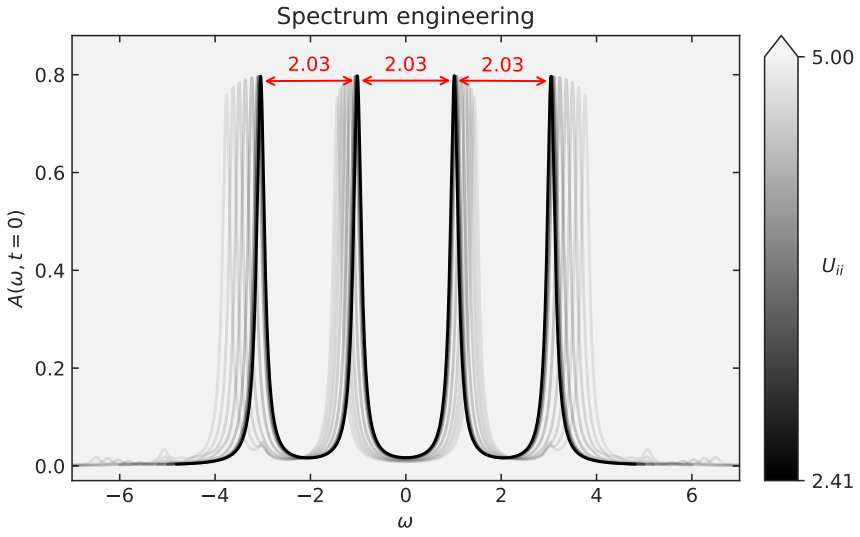

Fig. 3.2 Equilibrium spectral function $A(\omega)$ on site 0.

3.1.2 Why the spectral function may not be a good choice for small systems

In Fig. 3.3, we see the total energy of the spectrum engineered QD over time after being subjected to a light pulse of varying frequencies ω. As expected, for low values of ω, no electrons can be excited over the Mott gap and thus, no energy from the light pulse is absorbed. At $\omega = 2.00$, we see an energy increase as the light is now energetic enough to promote an electron into the upper Hubbard band.

Rather unexpectedly however, we see no energy gain at $\omega = 4.00$, meaning the first transition shown in Fig. 3.1 seems not to occur.

One possible explanation for this may be that the spectral functions we are using are not truly representative of the transitions between the eigenstates of our system. As briefly explained in section 1.2.6, we compute spectral functions by adding an electron/hole to the system, letting it propagate for a fixed time, then removing it again, and evaluating the overlap of this system with an unmodified one. Thus the spectral function shows us transitions between systems with electron numbers differing by one. For large systems with many electrons, adding or removing a single electron has an insignificant effect on its eigenenergy spectrum, and thus it will be equal to the spectral function. However, the effect may no longer be negligible for a small 2x2 site system like our QD. Meaning that the one-particle spectrum we see in Fig. 3.2 may not accurately represent the optical transitions possible in the QD.

It may be possible to remedy this with the use of Loschmid spectra, which do not suffer from the same issues in small systems [14]. However the implementation of these will have to wait for a future work.

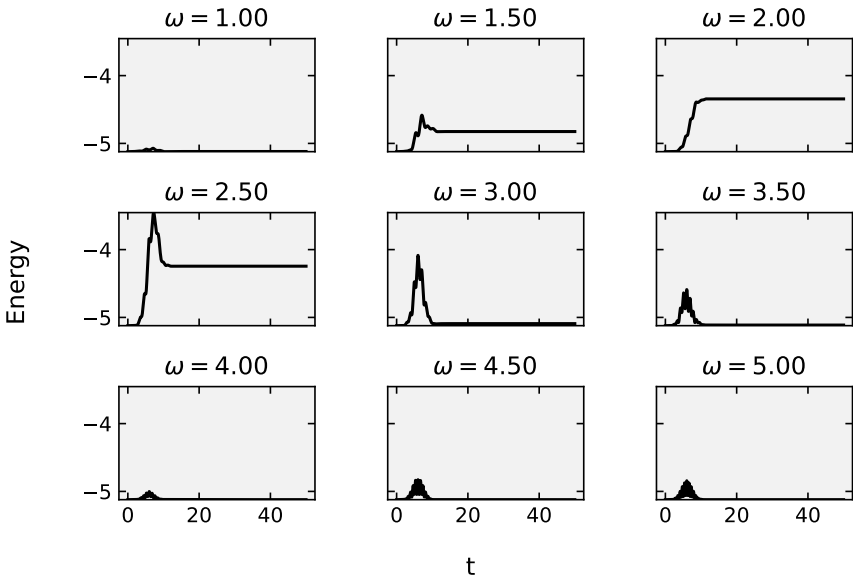

Fig. 3.3 Total energy in isolated QD system after interaction with light pulse at $t = 6$ for various frequencies ω.

3.2 Isolated Benzene

In order to verify if our new implementations work as intended, we compare the spectral functions we obtain for the isolated benzene ring with the one obtained by F. Hörbinger via exact diagonalisation of the PPP model [12]. We find that our results shown in Fig. 3.4 match those from [12] up to three significant figures after conversion into the appropriate units. Thus we can be reasonably confident that our implementation works for the isolated Benzene system.

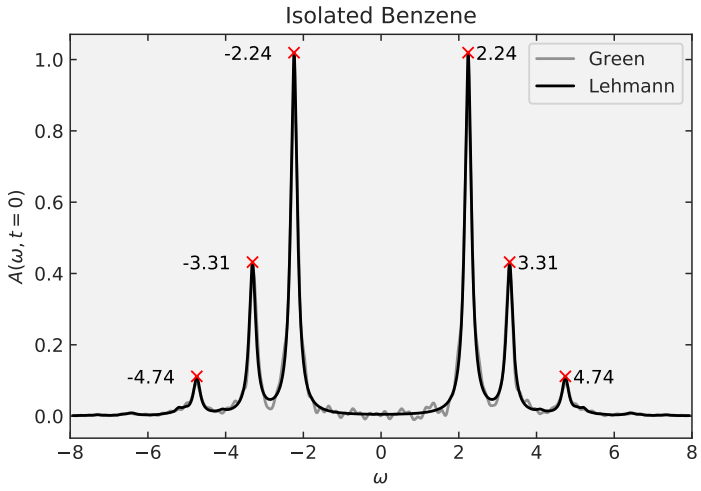

Fig. 3.4 Spectral function of isolated benzene with peak energies in agreement with results from [12] Parameters: $U = 3.96$, $a = 0.3$, $t_0 = 0$, broadening-factor $\epsilon = 0.1$

Additionally, we can also see from Fig. 3.4 that both the Lehmann spectrum and the spectral function obtained via the Fourier transformation of the Green's function produce comparable results, the only differences being the "noise" introduced in the Greens function spectrum due to the Fourier transform. This could be suppressed further by tweaking the broadening factor and the zero-padding of the domain, as briefly described in 1.2.6.

3.3 Coupled System

3.3.1 Testing

Before we investigate the effects of increasing the coupling strength between the two systems, we verify that if the hopping amplitude $v_c = 0$, the spectra on the individual sites remain unchanged. For the coupled system, calculating the Lehmann spectrum is no longer an option as memory becomes a limiting factor; instead, we resort to using the Green's function method.

This is indeed the case, as can be seen when comparing Fig. 3.5 with the spectra in Fig. 3.2 and Fig. 3.4. The slight variations being due to a difference in parameters used to perform the Fourier transformation.

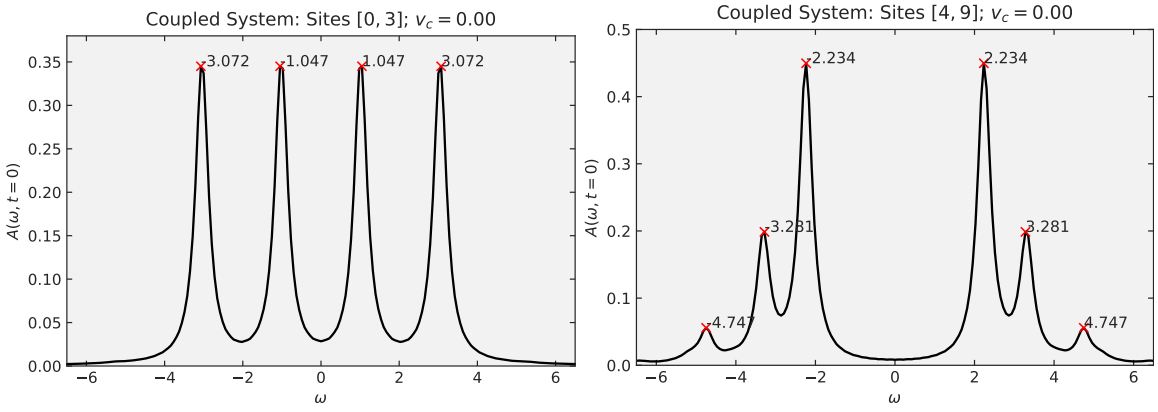

Fig. 3.5 Spectral function of all the sites of the coupled system with the coupling parameter turned off, $v_c = 0$. These spectra should be identical to those in Fig. 3.2 and Fig. 3.4

3.3.2 Dependence of the spectrum on the coupling strength

Fig. 3.6 and Fig. 3.7 show how the spectrum changes on each site as the coupling strength v_c between the QD and the benzene ring increases. Notice that the symmetry of the geometry is preserved, as all QD sites show the same spectra. The benzene site pairs 5, 9 and 6, 8 also each share identical spectra since they are symmetric about site 4, which is the one coupled to the QD.

In the spectrum of site 4 in Fig. 3.7, it is particularly evident that for larger v_c, the lower bands (below $\omega = 0$) become hybridised, meaning that the energy levels from the isolated systems shift towards each other, creating a new state. The reason this only happens for the lower bands has to do with the symmetry of the systems being broken upon allowing hoppings between the QD and benzene.

Another interesting effect that can be seen in Figs. 3.6 and 3.7 is that as v_c increases, the spectra experience a slight shift in energy. For the QD, the shift is towards lower energies, and for benzene, it is in the opposite direction. A possible explanation for this is given in 3.3.5.

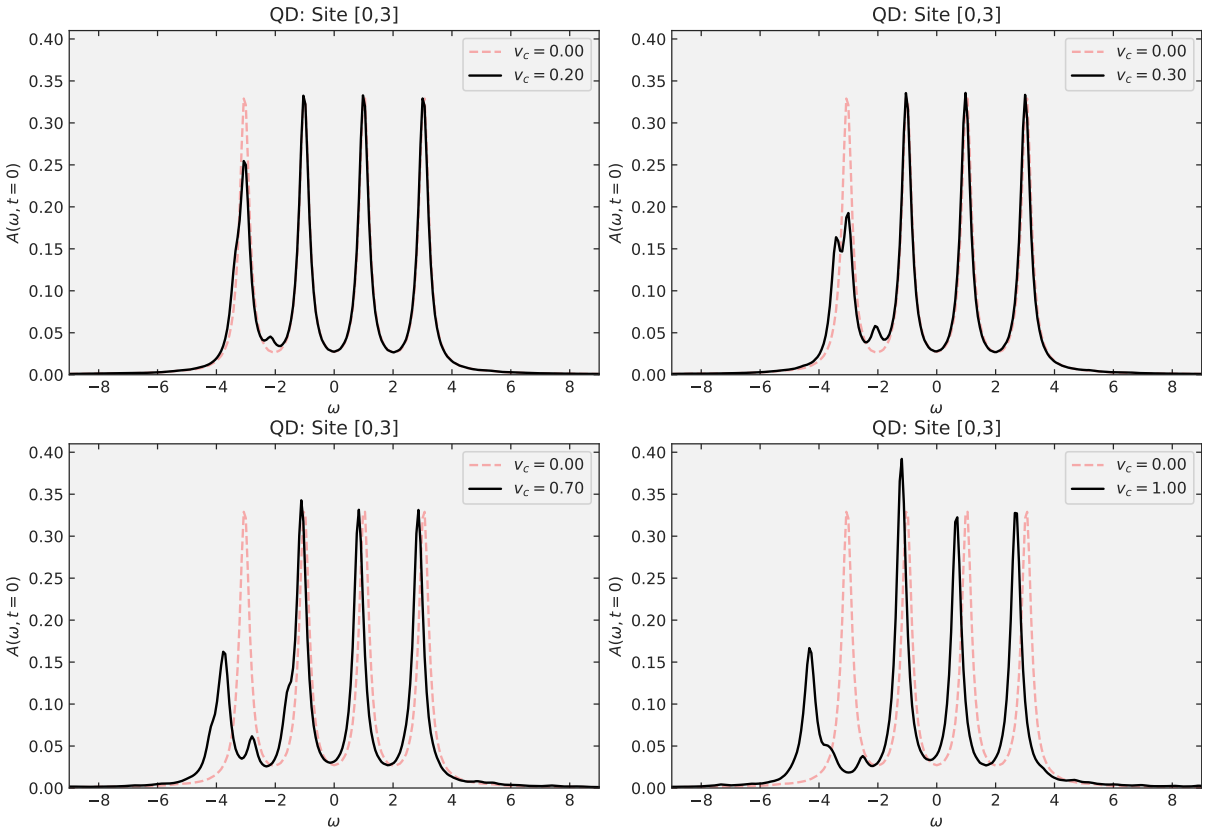

Fig. 3.6 Changes in the spectral function of the QD with increasing coupling v_c to the benzene ring

3.3.3 Interaction energy and impact ionisation

Ideally, we would like to investigate the changes in interaction energy on the QD and the benzene ring separately; however, because all the calculations happen in the state basis, and the interaction energy depends on multiple sites, calculating the observable on a particular set of sites is non-trivial. In the state basis, each basis vector is a state of the entire system, and thus all sites are always involved, making it impossible to separate which sites the contributions come from without a change of basis. Performing a transformation into the site basis is outside the scope of this work; thus, we will only be looking at the interaction energy of the system as a whole.

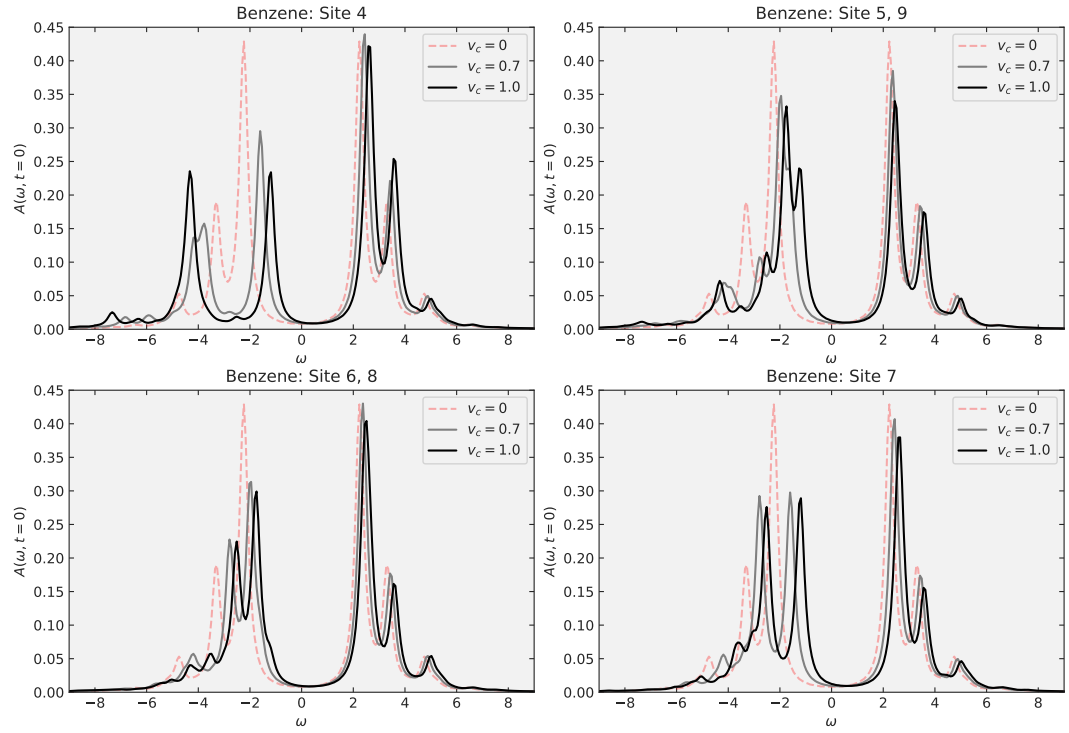

Fig. 3.7 Changes in the spectral function of the benzene ring with increasing coupling v_c to the QD

Fig. 3.8 shows the interaction energy $\langle \hat{E}_{\text{int}} \rangle$ for a light pulse with $\omega = 2.00$ and $\omega = 4.00$. Once without coupling the QD to benzene ($v_c = 0.00$) and once with strong coupling ($v_c = 1.00$). The two graphs with $v_c = 0.00$ are very similar to the total energy graphs seen in the QD system in Fig. 3.3. Like before, we see energy transfer at $\omega = 2.00$, but no permanent energy transfer from the light pulse to the system at $\omega = 4.00$, which indicates that no electrons are being promoted to the highest energy level.

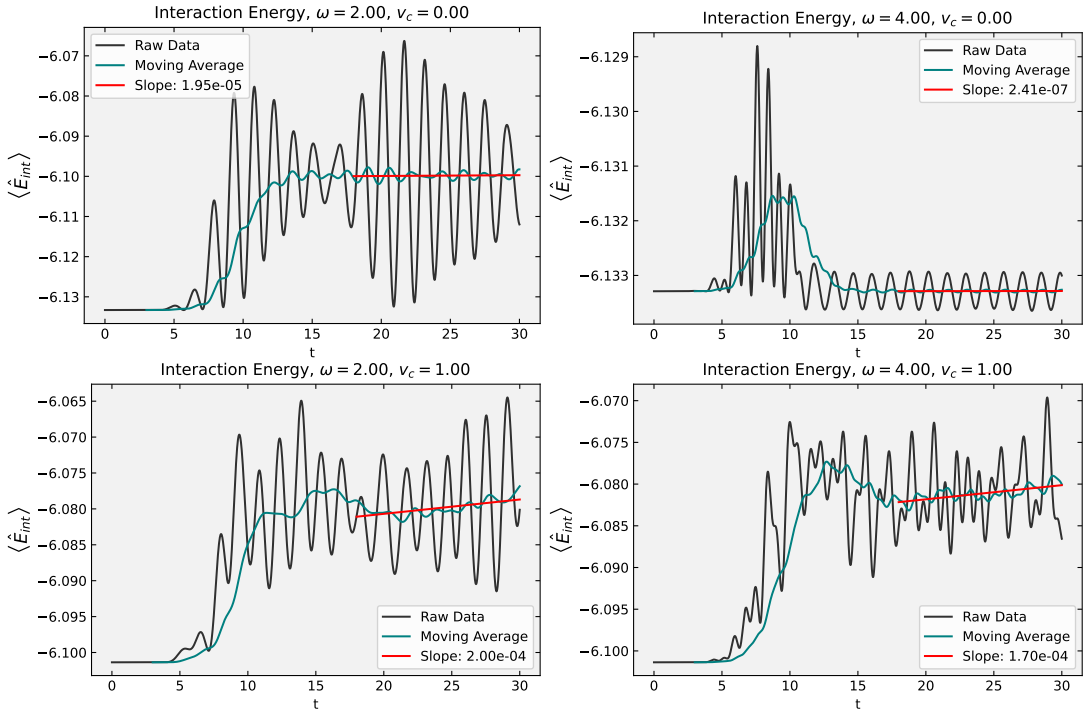

Fig. 3.8 Interaction energy of coupled system after excitation with light pulse. Shown with strong and without coupling between the QD and benzene.

Interestingly when $v_c = 1.0$, we see that for $\omega = 4.00$, there is an energy transfer and a steady rise in Interaction energy, even after the pulse has fully decayed, which should generally be an indicator of impact ionisation. Unfortunately, because we can not look at $\langle \hat{E}_{\text{int}} \rangle$ on a site-wise basis, we can not tell where this effect occurs. However, is look at the occupation numbers per site and attempt to draw conclusions from that.

3.3.4 Expected occupation number per site over time

Even though we can not study the interaction energy on each site individually, it is possible to compute the site-wise occupation numbers $\langle \hat{n}_i \rangle$ their evolution over time.

In Fig. 3.9, we see that for our system, which initially has 1 electron on each site, the electrons oscillate between sites 0 and 3 periodically. For $\omega = 4.00$, this oscillation lasts only as long as the pulse duration, but for $\omega = 2.00$, it persists since energy was permanently transferred from the pulse to the system. This is consistent with what was observed in Fig. 3.8.

We do not see any changes in occupations numbers on sites 1 and 2 due to the symmetry show in Fig. 2.2. Because the hopping between sites 0 and 3 is set to $v_d = 0$, all electrons moving between the two sites must pass through sites 1 and 2. In addition, because the light pulse hits the QD at a 45° angle with respect to the lattice, both vertical and horizontal hopping directions experience the same component of the electric field. Due to this, any electrons received from site 1 are immediately passed onto site 3 and vice versa, resulting in sites 1 and 2 having no occupation number changes. The time evolved occupation numbers for the benzene sites are not shown in Fig. 3.9 because they are constant at $\langle \hat{n}_i \rangle = 1$, because at $v_c = 0$, they do not interact with the light pulse.

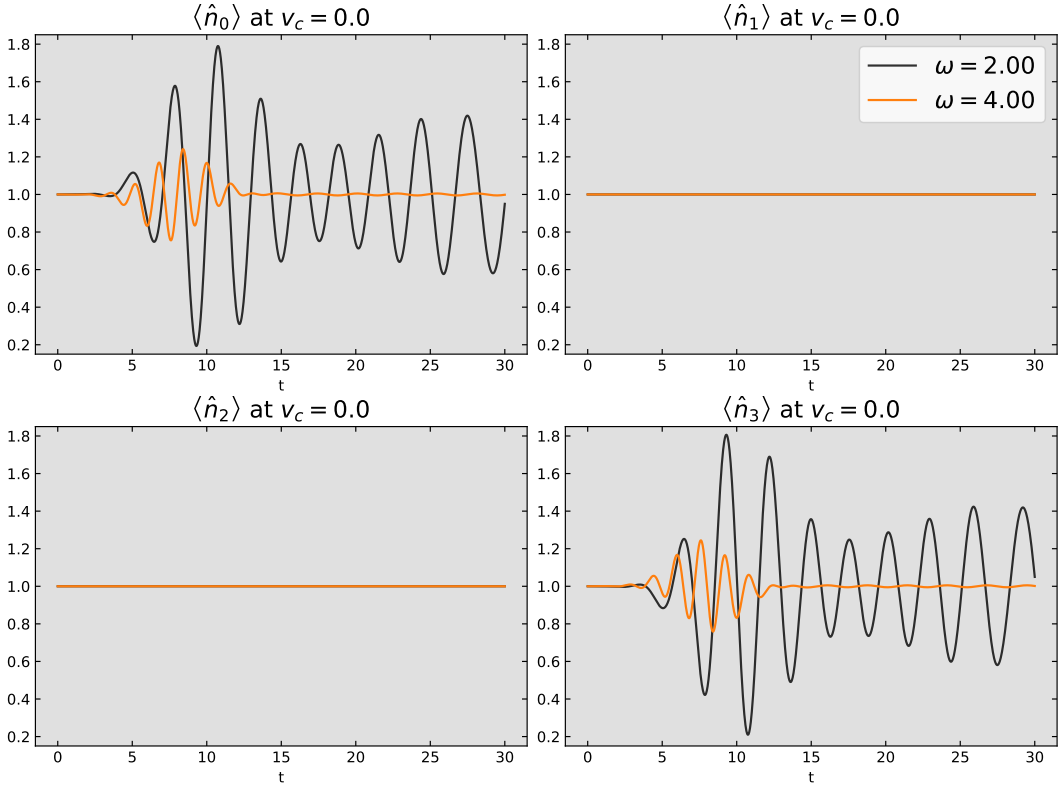

Fig. 3.9 Occupation numbers of QD sites as a function of time at two different light pulse frequencies. Because $v_c = 0.00$ and the benzene ring does not directly interact with the light pulse, all the occupation numbers of the benzene sites remain constant at 1.00 and thus are not shown in this figure.

When we increase the coupling strength v_c, electrons can flow between the QD and the benzene ring. Fig. 3.10 and Fig. 3.12 show the expected occupation numbers for $v_c = 0.30$ and $v_c = 1.00$ respectively. The figures are laid out to reflect the geometry of the coupled system, like the diagram in Fig. 2.5 turned 90° clockwise. Note that the y-axis scaling is different on the QD sites compared to the benzene sites since the occupation changes are smaller on benzene.

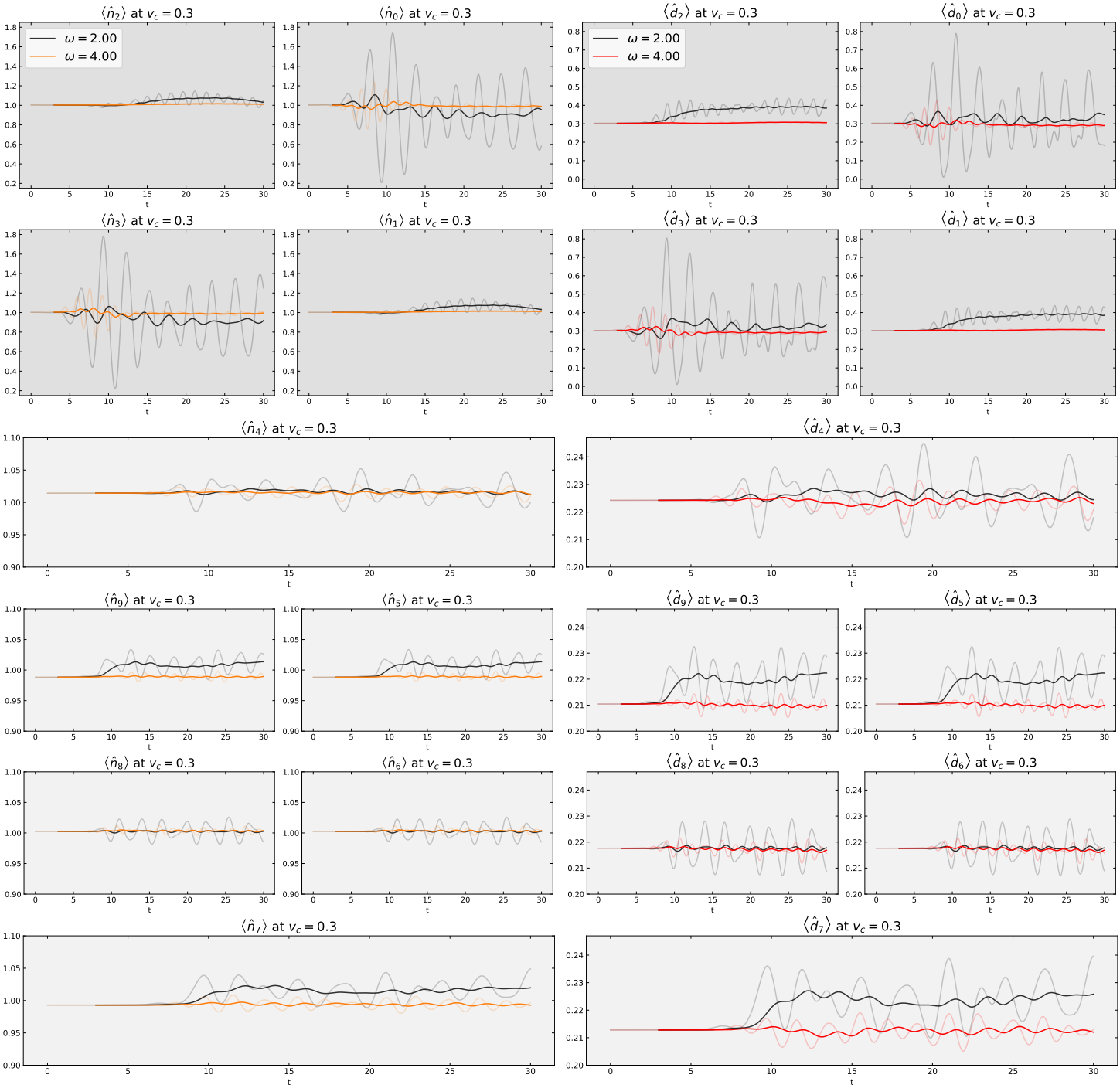

Fig. 3.10 Expectation of occupation numbers for the coupled system at $v_c = 0.3$. Darker lines are moving averages of the raw data shown in a lower opacity.

Fig. 3.11 Expectation of double occupation numbers for the coupled system at $v_c = 0.3$.

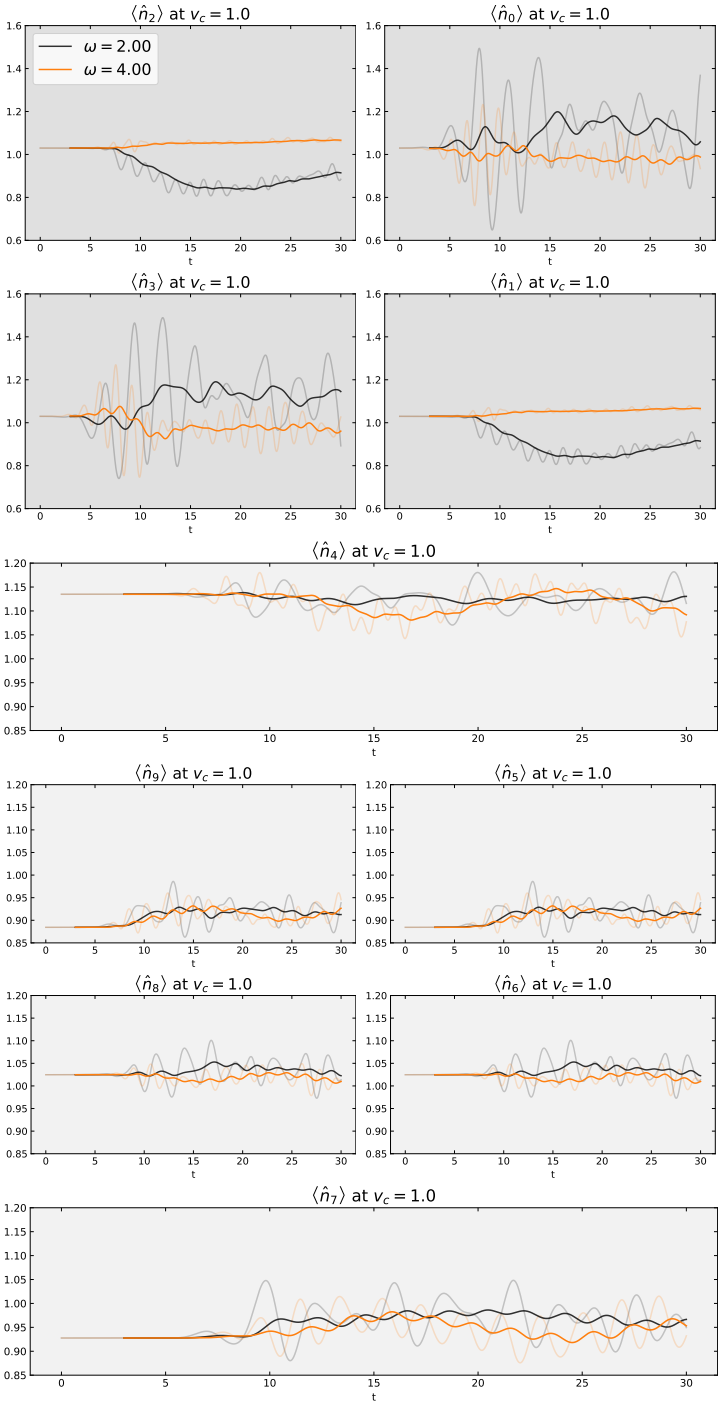

Fig. 3.12 Expectation of occupation numbers for the coupled system at $v_c = 1.0$. Darker lines are moving averages of the raw data shown in a lower opacity.

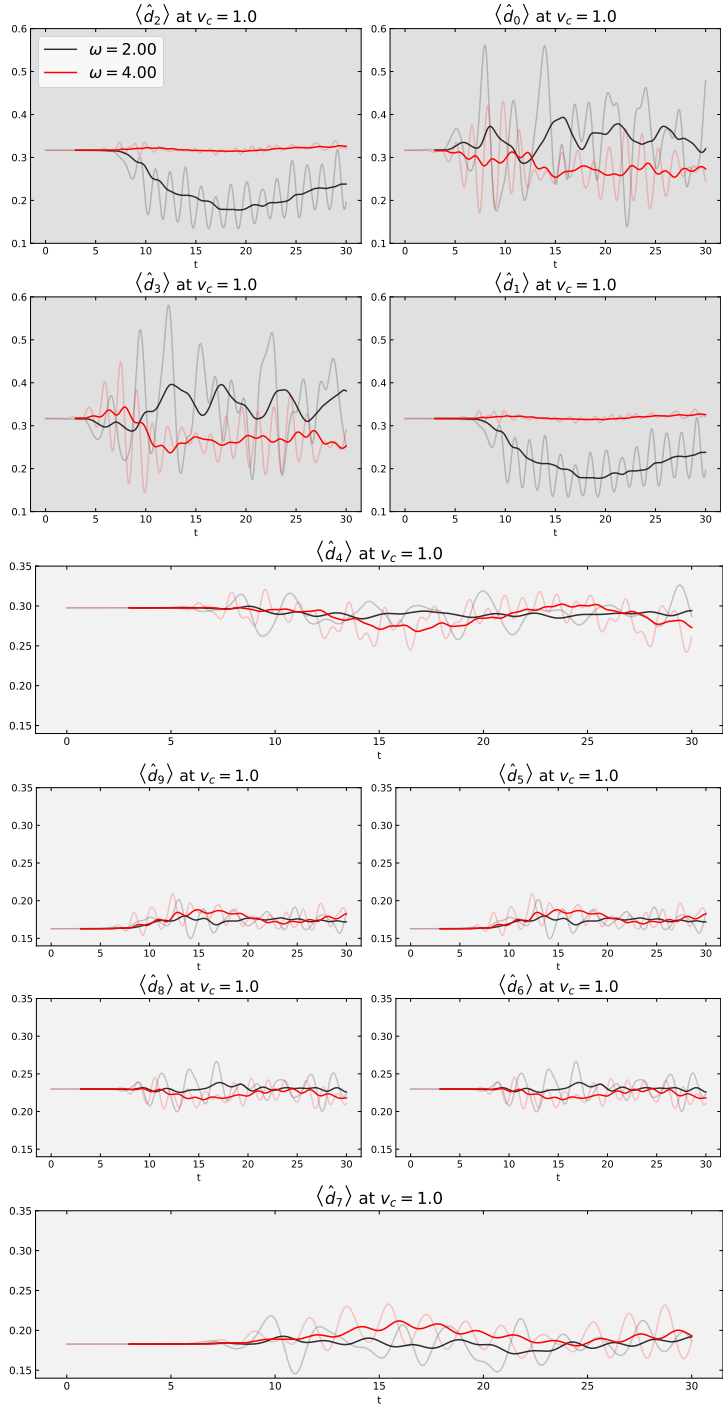

Fig. 3.13 Expectation of double occupation numbers for the coupled system at $v_c = 1.0$.

Fig. 3.10, in particular, reveals significant occupation increases on the benzene ring sites $7, 5$ and 9 at $\omega = 2.00$. Moreover, in Fig. 3.11, we see that from $t = 20$ onward, there is a steady rise in double occupation on those sites as well. Even though section 2.1.2 pointed out why double occupation is no longer a good measure for impact ionisation, seeing this steady increase after the pulse has decayed is still a weaker indication that impact ionisation may be taking place on the benzene ring.

3.3.5 Electron transfer between QD and benzene

In order to get a clearer picture of the electron currents between the QD and benzene subsystems than the site-wise occupation numbers from the previous section can provide, we calculate the sums of occupation number expectation values on all QD and all benzene sites. This allows us to study the net electron transfer between the two coupled systems.

All changes in the expected occupation numbers are calculated with respect to their occupation numbers at half-filling. This means that for the QD, 4 electrons were subtracted off the occupation number, and 6 electrons were subtracted from the occupation number of the benzene ring.

$$\begin{aligned} \langle \Delta \hat{n}_{\mathrm{QD}} \rangle (t) &= \left(\sum_{i=0}^{3} \langle \hat{n}_i \rangle (t) \right) - 4 \\ \langle \Delta \hat{n}_{\mathrm{benz}} \rangle (t) &= \left(\sum_{i=4}^{9} \langle \hat{n}_i \rangle (t) \right) - 6 \end{aligned} \tag{3.1}$$

Fig. 3.14 shows that, as expected, the total number of electrons is conserved and that for $v_c = 0.30$ and $\omega = 2.00$, there is a clear flow of electrons from the QD to the benzene ring, even after the pulse has fully decayed. This flow of electrons from the QD to benzene from roughly $t = 16$ onward coincides with the possible impact ionisation seen in the previous section. Because simply having more electrons on the benzene ring will lead to more double occupations, we can not clearly say which parts of the double occupancy increases are due to impact ionisation and which are due to the electron currents.

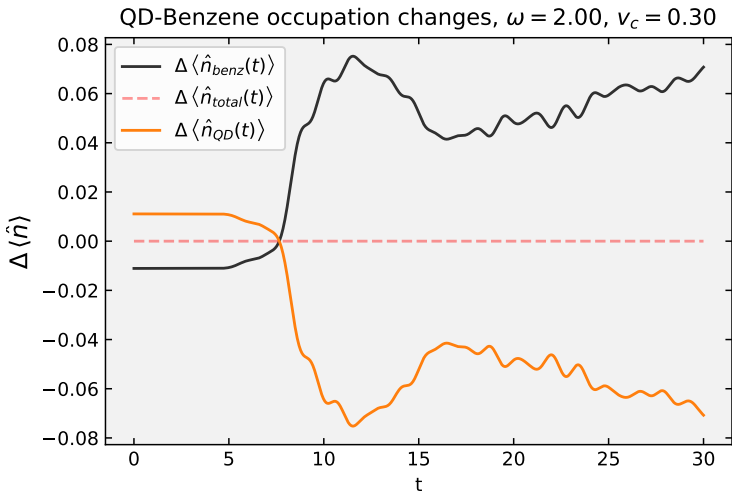

Fig. 3.14 Changes in expected occupation number between QD an Benzene over time.

Fig. 3.15 shows the occupation number changes on benzene for various coupling strengths. In addition to again seeing an increases in occupation after the pulse, there is also clear dependence of the occupation numbers at $t = 0$ on the coupling strength. This makes sense because at $t = 0$ the system is in its ground state and for this calculation the on-site Coulomb interaction term U_{ii} was chosen differently on QD sites and on Benzene sites. With $U_{ii}^{\mathrm{QD}} = 2.406$ and $U_{ii}^{\mathrm{Benz}} = 3.962$,

the energy cost of moving electrons form benzene to the QD is outweighed by the energy savings of having less electrons undergoing Coulomb interactions on the benzene ring, thus in the ground state $\Delta \langle \hat{n}_{\text{Benz}} \rangle < 0$ for $v_c > 0$.

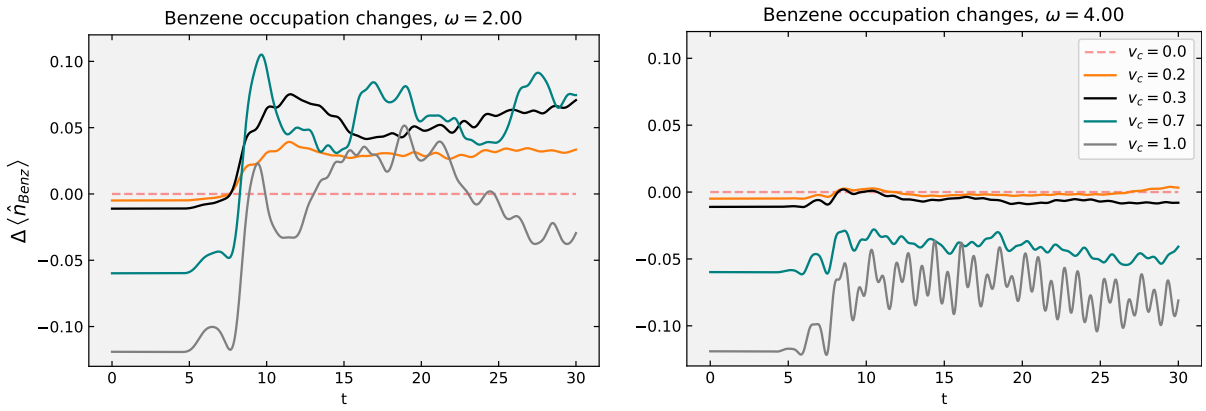

Fig. 3.15 Changes in expected occupation numbers for the benzene-subsystem at pulse frequencies $\omega = 2, 4$ for various coupling strengths v_c.

This also explains the shifting of the QD and benzene spectra with changing v_c in Figs. 3.6 and 3.7. The reduction in benzene's occupation numbers in the ground state can be seen as due to the up-shift in its energy levels, and because the energy levels in the QD are shifted downwards the ground state occupation increases.

3.4 Conclusion

In this work, we attempted to simulate an experimentally realisable system of a quantum dot coupled to a benzene ring and investigated its behaviour under photoexcitation by a light pulse, particularly in search of impact ionisation. However, the desired effects could not be clearly demonstrated. The final result is complicated because impact ionisation could not be uniquely identified in any single part of the system; instead, we see a mixture of effects on both the quantum dot and the benzene ring. Partially due to impact ionisation and partially due to charge transfer, which for now seem inseparably connected with each other. Further developments in the methodology for analysing this system will be needed to better understand the true mechanisms at work.

Bibliography

[1] Sven Rühle. Tabulated values of the shockley–queisser limit for single junction solar cells. *Solar Energy*, 130:139–147, 2016.

[2] Michael Innerberger. Modeling of solar cells by small hubbard clusters. Bachelor thesis, Technische Universität Wien, Sep 2017.

[3] Paul Worm. Impact ionization and non-equilibrium spectral functions from exact diagonalization of the hubbard model. Bachelor thesis, Technische Universität Wien, Jan 2018.

[4] Paul Prauhart. Spectral weight shift and enhancement of impact ionization in hubbard clusters with disorder and further neighbour hopping. Bachelor thesis, Technische Universität Wien, 2018.

[5] Paul Worm. Effect of phonons on impact ionization in small hubbard clusters. Project thesis, Technische Universität Wien, Nov 2018.

[6] Hai Wang, Erik R. McNellis, Sachin Kinge, Mischa Bonn, and Enrique Cánovas. Tuning electron transfer rates through molecular bridges in quantum dot sensitized oxides. *Nano Letters*, 13(11):5311–5315, 2013. PMID: 24093529.

[7] Philipp Werner, Karsten Held, and Martin Eckstein. Role of impact ionization in the thermalization of photoexcited mott insulators. *Phys. Rev. B*, 90:235102, Dec 2014.

[8] Hideo Aoki, Naoto Tsuji, Martin Eckstein, Marcus Kollar, Takashi Oka, and Philipp Werner. Nonequilibrium dynamical mean-field theory and its applications. *Rev. Mod. Phys.*, 86:779–837, Jun 2014.

[9] Wilhelm Magnus. On the exponential solution of differential equations for a linear operator. *Communications on Pure and Applied Mathematics*, 7(4):649–673, 1954.

[10] Anna Kauch, Paul Worm, Paul Prauhart, Michael Innerberger, Clemens Watzenböck, and Karsten Held. Enhancement of impact ionization in hubbard clusters by disorder and next-nearest-neighbor hopping. *Phys. Rev. B*, 102:245125, Dec 2020.

[11] Robert J Bursill, Christopher Castleton, and William Barford. Optimal parametrisation of the pariser–parr–pople model for benzene and biphenyl. *Chemical Physics Letters*, 294(4):305–313, 1998.

[12] Felix Hörbinger. Exact diagonalization of the pariser-parr-pople model. Bachelor thesis, Technische Universität Wien, Mar 2015.

[13] A. Franceschetti, J. M. An, and A. Zunger. Impact ionization can explain carrier multiplication in pbse quantum dots. *Nano Letters*, 6(10):2191–2195, 2006. PMID: 17034081.

[14] Clemens Watzenböck, Markus Wallerberger, Laurenz Ruzicka, Paul Worm, Karsten Held, and Anna Kauch. Photoexcitations in the hubbard model – generalized loschmidt amplitude analysis of impact ionization in small clusters, 2021.